

A Conserved Glutamate Residue Exhibits Multifunctional Catalytic Roles in D-Fructose-1,6-bisphosphate Aldolases*

Received for publication, August 9, 2001, and in revised form, December 21, 2001
Published, JBC Papers in Press, January 4, 2002, DOI 10.1074/jbc.M107600200

Amal Maurady[‡], Alexander Zdanov[§], Danielle de Moissac[‡], Danielle Beaudry[¶],
and Jurgen Sygusch^{‡||}

From the [‡]Department of Biochemistry, University of Montreal, CP 6128, Station Centre Ville, Montréal, Québec H3C 3J7, Canada, the [§]NCI-Frederick Cancer Research and Development Center, National Institutes of Health, Fort Detrick, Frederick, Maryland 21702, and the [¶]Department of Biochemistry, University of Sherbrooke, 3001, 12ieme Ave. Nord, Fleurimont, Québec J1H 5N4, Canada

The aldolase catalytic cycle consists of a number of proton transfers that interconvert covalent enzyme intermediates. Glu-187 is a conserved amino acid that is located in the mammalian fructose-1,6-bisphosphate aldolase active site. Its central location, within hydrogen bonding distance of three other conserved active site residues: Lys-146, Glu-189, and Schiff base-forming Lys-229, makes it an ideal candidate for mediating proton transfers. Point mutations, Glu-187 → Gln, Ala, which would inhibit proton transfers significantly, compromise activity. Trapping of enzymatic intermediates in Glu-187 mutants defines a proton transfer role for Glu-187 in substrate cleavage and Schiff base formation. Structural data show that loss of Glu-187 negative charge results in hydrogen bond formation between Lys-146 and Lys-229 consistent with a basic pK_a for Lys-229 in native enzyme and supporting nucleophilic activation of Lys-229 by Glu-187 during Schiff base formation. The crystal structures also substantiate Glu-187 and Glu-189 as present in ionized form in native enzyme, compatible with their role of catalyzing proton exchange with solvent as indicated from solvent isotope effects. The proton exchange mechanism ensures Glu-187 basicity throughout the catalytic cycle requisite for mediating proton transfer and electrostatic stabilization of ketamine intermediates. Glutamate general base catalysis is a recurrent evolutionary feature of Schiff base-forming aldolases.

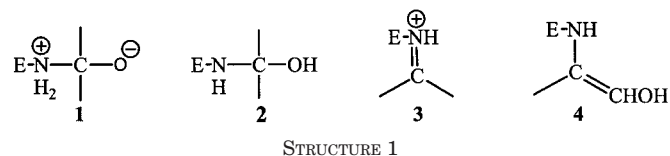
Fructose-1,6-bisphosphate aldolase (EC 4.1.2.13) is a ubiquitous glycolytic enzyme that catalyzes the reversible cleavage of D-fructose 1,6-bisphosphate to D-glyceraldehyde 3-phosphate and dihydroxyacetone phosphate, by an ordered uni-bi mechanism (1). Two classes of glycolytic aldolases can be distinguished that use different mechanisms to cleave the same substrate: Class I aldolases, present in higher eucaryotes and plants, catalyze their reaction mechanism via a Schiff base formation with a keto substrate whereas Class II aldolases, present in eubacteria and lower eucaryotes, require a divalent metal ion as a cofactor (2).

The catalytic mechanism of Class I fructose-1,6-bisphosphate aldolase has been well established in terms of reaction

mechanism intermediates (3), and the forward reaction can be represented by the following minimal reaction (Reaction 1)



consistent with the kinetic data (4), in which a lysine residue on the enzyme forms covalent intermediates (5) with the keto substrates, Fru-P₂,¹ Fru-P, and DHAP. In this forward reaction, Schiff base formation with Fru-P₂, E=DG, is thought to occur through transient formation of a dipolar carbinolamine-1 (4, 6) on the lysine nucleophile. Proton exchange with the dipolar carbinolamine results in the neutral species-2, which upon further protonation of the hydroxyl becomes dehydrated forming the protonated imine form of the Schiff base-3 (8). Proton abstraction of the Fru-P₂ O₄ hydroxyl initiates a rearrangement resulting in cleavage of the substrate C₃-C₄ bond and enamine formation in the active site yielding intermediate E-D·G (1, 9). Upon release of the glyceraldehyde 3-phosphate product, the enamine-4, E-D, is protonated (1) and forms a second Schiff base, E=DH, as shown in 3, which upon hydrolysis decomposes to the neutral carbinolamine species-2. Breakdown of the dipolar carbinolamine-1 then releases DHAP from the active site thereby regenerating the enzyme (Structure 1).



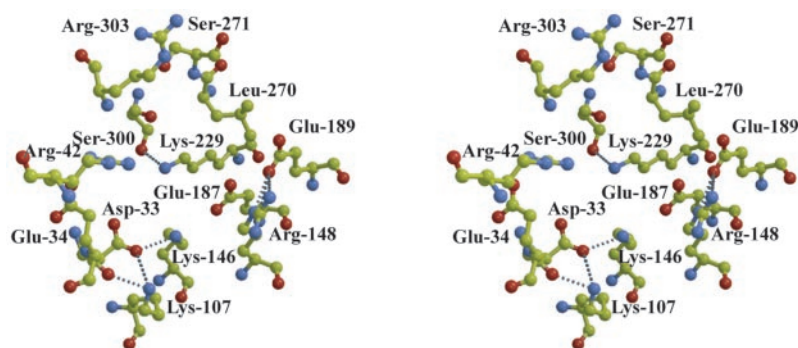
Evidence for covalent intermediates in equilibrium of muscle aldolase with Fru-P₂ and triose-Ps has been obtained by acid denaturation and precipitation (7, 9). Chemical trapping of intermediates in the forward steady state detected significant levels of Fru-P₂ ketamine (E=DG) and enamine (E-D) as well as minor levels of DHAP ketamine (E=DH) complexes (3).

* This work was supported by Grant-in-Aid MT-14768 from the Medical Research Council of Canada. The costs of publication of this article were defrayed in part by the payment of page charges. This article must therefore be hereby marked "advertisement" in accordance with 18 U.S.C. Section 1734 solely to indicate this fact.

|| To whom correspondence should be addressed. Tel.: 1-514-343-2389; Fax: 1-514-343-6463; E-mail: Jurgen.Sygusch@UMontreal.CA.

¹ The abbreviations used are: Fru-P₂, fructose 1,6-bisphosphate; Fru-P, fructose 1-phosphate; DHAP, dihydroxyacetone 1-phosphate; TEA-HAc, triethanolamine acetate; Tris-HAc, tris(hydroxymethyl)aminomethane acetate; E, enzyme; E=DG, the imine adduct between Fru-P₂ and E; E=DH, the imine adduct between DHAP and E; E-D, the enamine of DHAP on E; E-DG, the Michaelis complex of E with Fru-P₂; E-DH, the Michaelis complex of E with DHAP; E-D·G, the Michaelis complex of D-glyceraldehyde 3-phosphate with E-D; r.m.s., root mean square; r.m.s.d., root mean square deviation; KDPG, 2-keto-3-deoxy-6-phosphogluconate.

FIG. 1. **Stereoview of rabbit muscle aldolase active site.** Subunit orientation is shown looking into the β -barrel. Hydrogen bonds are indicated by dotted lines. Lys-229, which is situated at the bottom of the active site cleft, hydrogen bonds with Ser-300 while Asp-33 makes hydrogen bonds to both Lys-146 and Lys-107. Glu-187, although within potential hydrogen bonding distance of Lys-229, Lys-146, and Glu-189, does not participate in hydrogen bond formation. Both Arg-148 and Glu-189 are located at the active site surface and interact through hydrogen bonding.



Under equilibrium conditions in the presence of DHAP, the majority of covalent intermediate complexes are present as enamine ($E-D$) in mammalian aldolases whereas levels of ketamine complexes ($E=DH$) are by comparison substantially smaller albeit detectable.

Three-dimensional crystal structures of class I aldolases have been determined of muscle aldolase (10, 11), insect (12), and parasitic protozoa (13, 14). Class I aldolases are homotetramers composed of ~ 39 -kDa subunits. Folding of each subunit polypeptide chain corresponds to that of a β -barrel structure with the active site located deep in the β -barrel center and is shown in Fig. 1. Amino acid residues in the active site interior are highly conserved throughout evolution whereas peripheral active site residues differ among aldolases (15). The residue responsible for nucleophilic attack on the keto substrate in Schiff base formation has been identified as Lys-229 (5), situated in the active site interior (17), whereas Lys-107 on the active site periphery has been shown from protection experiments to bind the C_6 -phosphate of Fru- P_2 (16). Mutagenesis experiments of conserved active site residues have also implicated Arg-148 in C_6 -phosphate binding (24) whereas structural studies have shown that Ser-271 promotes C_1 -phosphate binding (17).

In contrast, the active site residues that are implicated in the proton transfers linking the covalent intermediates along the reaction trajectory have not been unambiguously identified. In the absence of structural data on covalent intermediate complexes, investigation of amino acid likely to be involved in proton exchanges has been guided by spatial proximity to Lys-229. Mutations of conserved residues Asp-33 and Lys-146, which are also within hydrogen bonding of each other, significantly comprised catalytic activity and, based on kinetic characterization, were postulated in mediating C_3-C_4 bond cleavage (18–20). In the structure of the Michaelis complex with DHAP, however, both residues are within hydrogen bonding distance of the incoming keto oxygen (17) suggesting rather roles in Schiff base formation. Indeed, point mutation Lys-146 \rightarrow Arg results in Schiff base formation becoming rate-determining (19). Alanine substitutions of active site residues, Glu-34 and Arg-42, by contrast do not significantly reduce activity or binding (24). Mutations of conserved residue Glu-187, adjacent to both Lys-146 and Lys-229 in the active site, significantly compromised activity and perturbed the rate of Schiff base formation of an aromatic inhibitor with Lys-146 (22). Structural data from the Michaelis complex of substrate bound to rabbit liver aldolase places Glu-187 within hydrogen bonding distance of both Fru- P_2 O_4 hydroxyl as well as Lys-229.² Structural studies performed with Fru- P_2 in complex with human muscle isozyme or an inactive point mutant, K146A, were, however, not unequivocal and did not allow definitive functional assignment of active site residues (23, 24).

The structural and enzymatic data alludes to a significant role by Glu-187 in the reaction mechanism of class I aldolase that warrants further investigation. A role by Glu-187 in catalyzing proton transfers would be consistent with its central location in the active site. Not only is Glu-187 within hydrogen bonding distance of possible proton donors, Lys-146 and Lys-229, but it is also within hydrogen bonding distance of a proton acceptor, conserved active site residue Glu-189. Functionality of Glu-187 was explored by assessing the impact of a series of point mutations that drastically diminish proton transfer capability. Isosteric point mutations, E187Q, E189Q, and K229M, and side-chain deletion mutants, E187A and E189A, were analyzed by combination of enzymological and crystallographic techniques. Activity profiling as a function of pH and solvent isotope effects were used to assay proton transfer capability while chemical trapping of intermediates in the presence of labeled [³²P]DHAP and [1-³²P]Fru- P_2 (3), and carbanion oxidation data were used to determine the formation of covalent intermediates in Glu-187 mutants. Structural studies on three point mutations, E187A, E187Q, and K229M, whose activities were significantly compromised, were also determined to assess active site integrity and possible conformational rearrangements. The structural and biochemical analysis indicates that Glu-187 is the base responsible for promoting cleavage of the C_3-C_4 bond in substrate and has a significant role, together with Lys-146, in turnover of cationic Schiff base intermediates. Indeed, a conserved glutamate residue is found in 2-keto-3-deoxy-6-phosphogluconate (KDPG) aldolase, which also possesses a β -barrel subunit fold, within hydrogen bonding distance of the active site lysine responsible for Schiff base formation and has been implicated in both Schiff base formation as well as bond cleavage (25).

MATERIALS AND METHODS

Enzyme Analysis—Expression and purification of recombinant rabbit muscle aldolase and corresponding point mutations were performed as reported previously (26). Purification was based on substrate affinity elution from carboxymethyl-Sepharose stationary phase and using gel filtration for protein clean up.

Kinetic Analyses—Aldolase cleavage assay was measured by following NADH oxidation at 340 nm at 22 °C using a coupled assay system, triose-phosphate isomerase and glycerol-3-phosphate dehydrogenase, and detected using a Lambda 2 spectrophotometer (PerkinElmer Life Sciences) (27). The rate of substrate cleavage was determined by measuring the decrease in absorbance/minute at 340 nm. Specific activity assays were initiated by addition of substrate to a cuvette containing aldolase made up in 100 mM TEA-HCl, pH 7.6, 1 mM EDTA, 0.42 mM NADH, and coupling enzymes 1 μ g/ml triose-phosphate isomerase and 10 μ g/ml glycerol-3-phosphate dehydrogenase. The cleavage rate of Fru- P_2 was measured over a substrate concentration range of 10 μ M to 1 mM Fru- P_2 , using 0.3 μ g in the case of the wild type enzyme, 10–300 μ g for point mutants E187A, E187Q, E189A, and E189Q, and 2 mg of enzyme for point mutation K229M. Kinetic parameters were determined from double-reciprocal plots. Aldolase concentration was determined by absorbance using extinction coefficient, ϵ_{280} (%) = 0.91 ml \cdot mg⁻¹ \cdot cm⁻¹. Activity profiles as a function of pH were performed using 50 mM Tris-HAc buffer at varying concentrations of Fru- P_2 to

² N. Blom, A. White, J. Allard, and J. Sygusch, manuscript submitted.

determine kinetic parameters, V_{\max} and K_m , as a function of pH. Measurements in all activity assays were made in duplicate. Estimated errors in kinetic parameters were on approximately $\pm 20\%$ of estimated value.

The enamine carbanion intermediate can be oxidized by hexacyanoferrate(III) and is quantitative with enamine concentration (28). The rate of hexacyanoferrate(III) reduction was followed by a decrease in absorption at 420 nm as previously described (26). Steady-state oxidation rates were measured in the presence of 1 mM Fru-P₂ whereas equilibrium oxidation rates were determined in the presence of 1 mM DHAP using 0.3 μg in the case of the wild type enzyme, 10–300 μg for point mutants E187A, E187Q, E189A, and E189Q, and 1 mg of enzyme for point mutation K229M. Estimated errors in oxidation rates were on average $\pm 20\%$ of estimated value.

To evaluate D₂O kinetic solvent isotope effects, enzyme activity measurements were performed in D₂O using 50 mM Tris-HAc buffer, pH 7.5, and the effect of D₂O on pH was corrected for. Substrate and Tris-HAc buffer was made up as a concentration in D₂O, and coupling enzymes were diluted in D₂O prior to usage. Together this amounted to less than a 5% reduction in D₂O concentration in the activity assay. Recombinant aldolase enzymes were dialyzed against three successive changes of D₂O for at least 1 h each until measured activity became stable. Enzyme dialyzed against similar three successive changes of H₂O was used for control.

Chemical Trapping of Reaction Intermediates—Covalent enzyme-substrate intermediates were characterized by acid precipitation and chemical lability of the precipitated species (3). The end-point assays used a 10- to 100-fold excess of substrate with respect to 0.5–1.5 nmol of enzyme. Protocols for determination of the concentration of the intermediates $E=DG$, $E=D$, and $E=DH$ were as previously reported (3, 7, 9). Recombinant rabbit muscle aldolase preparations were incubated with either labeled [³²P]DHAP (40–60 cpm/pmol) or [³²P]Fru-P₂ (55–65 cpm/pmol) at pH 7.5 in 50 mM TEA-HAc buffer at 20 °C. Labeled inorganic phosphate was estimated at ~ 0.1 – 0.2% of labeled Fru-P₂ and $\sim 10\%$ of labeled DHAP. To each reaction mixture, 100 μg of bovine serum albumin was added to minimize nonspecific losses of labeled intermediates. The concentration of labeled Fru-P₂ was 1 mM for native enzyme and 0.4 mM for mutant enzymes. Enzyme preparations were used fresh and corresponded to a maximal activity of 16 units/mg for native enzyme (see Table II below). Under these conditions, the native recombinant enzyme is maximally active and kinetically homogeneous (3). Imine and carbinolamine complexes of aldolase with Fru-P₂ and DHAP were isolated in the protein precipitate and recovered as Fru-P₂ and DHAP after mild acid extraction of the protein precipitate (3). P₁ produced in the acid quench is derived from the enamine intermediate (9) and was quantitatively extracted into 2-methyl-1-propanol as the acid molybdate complex (29). Precipitation of the reaction mixture was performed with cold 1 M trichloroacetic acid and centrifugation for 1–2 min at 4 °C. Extraction of the protein pellet with 0.5 N NaOH for 2 min at 37 °C released ³²P₁, and alkali label counts were used to calculate the concentration of ketamine, $E=DH$, whereas residual counts in the pellet reflected the concentration of ketamine, $E=DG$, in the forward reaction. Minimum incubation times were 3 s using labeled Fru-P₂ and 20 s with labeled DHAP to allow full conversion of DHAP gem diol form to the free keto form. In the forward steady-state reaction, 1 mM [³²P]Fru-P₂ concentration was used with native recombinant enzyme to ensure that total Fru-P₂ concentration remained in excess with respect to enzyme over the 3-s assay interval. Controls performed used identical protocols with enzyme omitted.

Kinetic trapping experiments using mutant aldolases were conducted under identical conditions as the native recombinant enzyme. To assess steady-state levels in the forward reaction in E187A and E187Q mutants, trapping experiments were also carried out for 1 and 20 min, respectively. Chase solutions diluted carrier 10-fold, except in the case of forward reaction with Glu-187 mutants where the dilution was 25-fold. All kinetic trapping experiments were performed in triplicate from at least two different enzyme preparations, and results were averaged. Fluctuation in replicates was 1–2% of average value for a given preparation. Backgrounds were significantly lower in precipitates used to estimate ketamine populations compared with enamine populations, which are derived from supernatants that had larger background counts due to the presence of inorganic phosphate. Errors in intermediate populations were estimated at $\sim 15\%$ and $\sim 25\%$, respectively, for ketamine and enamine populations based on values obtained from different enzyme preparations and are shown below in Tables IV and V. Rate constants, k , characterizing time taken to reach steady state in Glu-187 mutants, were obtained by solving the relation $A_t = A_\infty[1 - \exp(-kt)]$, where A_t and A_∞ represent intermediate concentrations at

time t and $t = \infty$, respectively, such that,

$$k = -\frac{1}{t} \ln\left(\frac{A_\infty - A_t}{A_\infty}\right) \quad (\text{Eq. 1})$$

Triose-P isomerase and glycerol-P dehydrogenase used for triose-P detection in the steady-state forward reaction were increased with respect to concentrations used previously (3). In commercial preparations of triose-P isomerase (Roche Molecular Biochemicals), lag in triose-P turnover correlated with higher ketamine ($E=DG$) accumulating on the native enzyme. Increasing concentration of triose-P trapping enzymes to 3 \times of previous values minimized this accumulation. Even greater concentrations had no further significant effect.

Crystallization and X-ray Diffraction Data Collection—Crystals for recombinant mutant aldolases were obtained using vapor diffusion technique and/or batch crystallization (10). Crystal growth experiments using mutant Glu-187 proteins were also performed in microgravity using a step gradient liquid-liquid diffusion method (31). Protein crystallization experiments were performed on NASA Shuttle flight STS-86 and involved a sliding block technology that superposes, following block activation, two fluid half-wells that were initially separated. The initial protein solution contained 40% saturated ammonium sulfate and 10 mg/ml concentration of protein and was allowed to equilibrate for 10 min in microgravity against an equal solution (150 μl) of 50% saturated ammonium sulfate to induce nucleation and then transferred to a second solution containing 43% saturated ammonium sulfate. This technology is best performed in a microgravity environment, because it is based on free liquid-liquid interface diffusion of a precipitant solution against a protein solution. Superposition allows diffusion to occur, inducing nucleation and crystal growth. Ground control crystals for both mutants were grown by batch method on the ground as described previously (10). In each case, this exemplified protein crystal growth under best laboratory conditions.

Protein crystals were recovered for both Glu-187 mutants at the end of the 10-day microgravity mission. Microgravity-grown crystals of mutant E187A yielded a visible diffraction pattern to 2.1-Å resolution compared with best ground controls, which diffracted to only 2.4-Å resolution. Crystals of mutant E187Q did not show substantial resolution difference with respect to growth in a microgravity environment. Crystals grown of both mutants independent of gravitational environment attained a maximum size of $\sim 1.2 \times 0.8 \times 0.2$ mm, were cut to 0.5-mm maximum dimension, and were mounted in glass capillaries for intensity data collection. Unit-cell parameters and crystal data are summarized in Table I below. All data were collected from a single crystal using a Siemens X-100 multiwire detector mounted on a Rigaku RU-200 rotating anode generator. Data reduction was performed with the XGEN package (32). Crystals of K229M diffracted to 2.6-Å resolution and were grown by batch method in the laboratory.

Structure Determination and Refinement—Crystals of the mutant aldolases were isomorphous with native protein, having monoclinic space group P2₁, and mutant structures were solved by difference Fourier methods. Atomic coordinates from the native muscle aldolase structure, refined at 1.9 Å, were used to initiate refinement of the mutant structures. The initial model had solvent molecules, DHAP, and the C-terminal region removed. All refinements, map calculations, and geometric analyses were carried out by simulated annealing (33) using X-PLOR version 3.1. The initial model was subjected to rigid-body refinement using X-PLOR resulting in an R -factor for the E187A, E187Q, and K229M of 39, 32, and 34%, respectively, and was followed by several rounds of simulated annealing to remove any bias from the initial model. Each round of simulated annealing consisted of initially heating to 3000 K and then slowly cooling to 300 K in increments of 250 K and using 500 steps of 0.5 fs each to equilibrate at each annealing temperature. Resolution of the starting model used was 2.5 Å for E187A and E187Q mutants and 2.9 Å for the K229M. Higher resolution shells were gradually added in subsequent refinement cycles. Electron density maps were calculated with structure factor coefficients $2|F_o| - |F_c|$ and $|F_o| - |F_c|$. The program O was used for electron density interpretation (34). Following each cycle of refinement, fit by amino acid residues to the electron density was verified using OOPS (35). Water molecules were gradually included during each refinement cycle and were selected from spherical peaks having electron density greater than 2.5σ . The trace of the C-terminal sequence (residues 344–363) was through regions of weak electron density on initial maps but was readily followed once sufficient water molecules had been added (36). The final map showed clear connected electron density in all tetramer subunits, and final refinement statistics are summarized below in Table I. In the mutant E187A where Lys-146 and Lys-229 exhibited dual conformations, side-chain occupancy was set to 0.5 in each conformer. A test

TABLE I
 Data collection and refinement statistics

Crystallographic data	E187A	E187Q	K229M
Space group	P2 ₁	P2 ₁	P2 ₁
Unit cell constants (a, b, c (Å))	165.97, 58.36, 86.95	164.32, 57.51, 85.36	164.24, 57.41, 85.05
β (degree)	103.164	102.66	102.65
Asymmetric unit	Tetramer	Tetramer	Tetramer
Resolution maximum	2.15	2.0	2.6
No. of total reflections	88,801	88,145	87,439
No. of unique reflections	56,675	81,034	48,198
Completeness ^a (%)	81	83	84
R _{sym} ^b (%)	7.7	6	10
R _{fac} ^c (%)	17.8	19.1	17.7
R _{free} ^d (%)	22.9	23.3	23.2
Resolution ^e (Å)	10–2.2	10–2.0	12–2.6
No. of reflections ^f	55,143	87,623	34,787
No. of atoms	17,409	17,107	15,586
No. of water molecules	3,498	3,500	2,189
No. of sulfate ions	0	2	2
r.m.s.d. bond lengths (Å)	0.011	0.008	0.011
r.m.s.d. angles (degree)	1.812	1.678	1.8
r.m.s.d. dihedral (degree)	22.1	21.5	22.4
r.m.s.d. improper (degree)	1.21	1.45	1.71

^a Completeness (%).

^b R_{sym} (%) = $\sum_{hkl} \sum_i |I_i(hkl) - \bar{I}_i(hkl)| / \sum_{hkl} \sum_i I_i(hkl)$, where I_i is the observed intensity of i th equivalent reflection hkl .

^c R_{fac} (%) = $\sum_{hkl} \|F_o(hkl) - |F_c(hkl)|\| / \sum_{hkl} F_o(hkl)$, crystallographic R -factor, where $|F_o|$ and $|F_c|$ are the observed and calculated structure factor amplitudes, respectively, of reflection hkl .

^d R_{free} (%) = $\sum_{hkl} \|F_o(hkl) - |F_c(hkl)|\| / \sum_{hkl} F_o(hkl)$, is the test reflection data set and 8% of all reflections, selected randomly.

^e Resolution range used in refinement.

^f Used for refinement.

reflection data set representing 8% of all reflections, selected randomly, was used for cross-validation during crystallographic refinement (37). All figures were prepared using programs BOBSCRIPT (38) and RASTER3D (39).

Quality of the Model—The quality of the refined structures was verified by the program PROCHECK (40) and root mean square (r.m.s.) deviations from ideal bond lengths and angles are shown in Table I. The program OOPS and Ramachandran plots of the final model were used to verify protein geometry and are summarized in Table I. The atomic coordinates for mutants: K229M, E187A, and E187Q are available from the Research Collaboratory for Structural Bioinformatics Protein Data bank (www.rcsb.org/pdb) deposited under accession codes 1EWE, 1EX5, and 1EWG, respectively.

RESULTS

Mutant Aldolase Activities—Kinetic parameters of the isosteric neutral point mutations E187Q and E189Q as well as point mutations E187A and E189A are shown in Table II. Comparisons with the native recombinant enzyme indicate significant changes in V_{max} with only relatively small changes in K_m at pH 7.6. Maximal activity of E187Q was reduced by a factor of 2.3×10^{-4} toward Fru-P₂ suggesting that this residue participates in formation and dissociation of reaction intermediates. A slightly higher activity, ~4-fold, in the point mutant E187A with respect to E187Q, was surprising. Loss in catalytic activity of mutants E189Q and E189A was small with practically no activity loss in the latter. The oxidation rates for the enamine carbanion intermediate, shown in Table III, reflect trends similar to those observed for catalysis; rates for Glu-187 mutants were significantly decreased whereas those for E189 mutants were considerably less affected. The oxidation rates for the incompetent K229M mutant reflects residual background activity, and, when taken into account, steady-state carbanion oxidation rates in Glu-187 mutants are comparable with those observed for catalytic activity. In contrast, equilibrium oxidation rates exceeded steady-state rates by more than 2-fold. Oxidation rates for E189 mutants are comparable with those of native enzyme, which are determined by release of the oxidized carbanion from the native enzyme (41).

The decrease in V_{max} in all point mutants could not be compensated for by changes in pH. The pH-activity profiles for Glu-187 mutants, shown in Fig. 2b, indicate with respect to

 TABLE II
 Kinetic parameters and solvent isotope effects of Fru-P₂ cleavage reaction for recombinant mutant aldolases of active site residues Glu-187, Glu-189, and Lys-229 assayed at pH 7.6

Enzyme	k_{cat}	K_m	D_2O k_{cat}^a
	s^{-1}	μM	
Native recombinant	42.2 ± 0.8	5.1 ± 1.9	2.7
E187Q	0.03 ± 0.003	13.4 ± 1.1	2.9
E187A	0.12 ± 0.015	6.2 ± 0.6	1.4
E189Q	1.69 ± 0.09	10.9 ± 1.5	2.6
E189A	36.9 ± 1.5	5.7 ± 1.1	3.7
K229M	<10 ⁻⁵	ND ^b	ND

^a Solvent isotope effect represented by ratio of $k_{cat}^{H_2O} / k_{cat}^{D_2O}$.

^b ND, not determined.

 TABLE III
 Carbanion oxidation rates for native and mutant enzyme · substrate complexes in presence of Fru-P₂ (1 mM) or DHAP (1 mM)

Enzyme	Fru-P ₂		DHAP	
	s^{-1}			
Native recombinant	3.35 ± 0.15		3.06 ± 0.15	
E187Q	0.06 ± 0.02		0.52 ± 0.08	
E187A	0.16 ± 0.03		0.44 ± 0.09	
E189Q	3.28 ± 0.15		2.35 ± 0.13	
E189A	1.93 ± 0.20		2.13 ± 0.17	
K229M	<0.03		<0.05	

native enzyme (Fig. 2a) a consistent loss of catalytic activity by several orders of magnitude over the entire pH interval (pH 5–10) with maximal activity displaced to acid pH. A similar shift in maximal activity can be seen for E189Q in Fig. 2c. The pH-activity profile observed for E189A in Fig. 2c is very similar to native enzyme and shows only a slight uniform loss in catalytic activity with respect to native enzyme. The mutation of the lysine residue responsible for Schiff base formation with the substrate eliminates the capacity of the enzyme to promote Schiff base formation. The K229M mutant measures essentially the background level of activity and has a rate of Fru-P₂ cleavage that is <10⁻⁶ of wild type.

The kinetic solvent isotope effects observed, also shown in Table II, were unchanged for the isosteric point mutants E187Q and E189Q with respect to native enzyme. The inverse

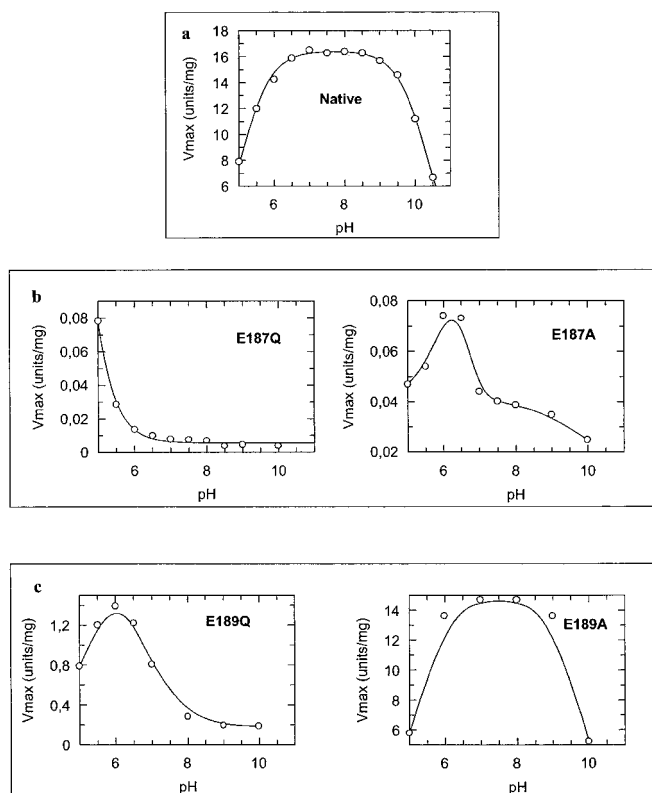


FIG. 2. pH activity profiles for native recombinant aldolase and site-directed point mutations. *a*, native enzyme profile; *b*, profiles for mutants E187A and E187Q; *c*, profiles of mutants E189A and E189Q.

kinetic solvent isotope effect observed for E187A in Table II corresponds to Glu-187 side-chain loss that has created a cavity and enabled a water molecule such as OH^- species to participate in catalysis. OH^- species have strongly inverse fractionation factors (42). The increase in the kinetic solvent isotope effect for E189A with respect to wild type of ~ 1.4 -fold is significant even though loss of the carboxyl side chain only very slightly decreased activity. The cavity created at the subunit surface by the Glu-189 \rightarrow Ala mutation would allow a water molecule to participate in catalysis. Solvation catalytic proton bridges can have significant fractionation factors in the transition state that produce sizeable secondary isotope effects (43). The increased kinetic solvent isotope effect in the E189A mutant falls within experimental error in the range of 1.5–4 expected for transition state proton transfers.

Intermediate Concentrations—Stoichiometries obtained for recombinant native aldolase and point mutants, E187A and E187Q, in the forward direction are shown in Table IV. Stoichiometries were corrected for background by subtracting counts of control reactions containing no enzyme from the experimental values. A net stoichiometry of 4 is consistent with full occupancy of all aldolase subunits by an intermediate and, from data in Table IV, indicates that Michaelis intermediates represent the large majority of enzymatic complexes in the forward direction. Stoichiometry of ketamine and enamine intermediates ($E=$ DG and $E=$ D) in the native enzyme differs from that reported in a previous study where the ketamine intermediate rather than enamine was the major covalent species (3). Taking into account only 10-fold isotopic dilution of the labeled species by carrier, reductions in covalent species upon chase were consistent with intermediate populations that are completely displaceable in the native enzyme. The very low concentration of chased intermediates indicates an absence of

slow interconverting enzymatic species and is characteristic of enzyme homogeneity. Treatment of the native recombinant enzyme with carboxypeptidase resulted in the expected enamine accumulation (1).

Stoichiometries of all intermediates for Glu-187 mutants, shown in Table IV, were reduced 10-fold compared with native enzyme in the forward direction. The increase in enamine stoichiometry upon prolonged incubation in both E187A and E187Q mutants indicates that steady-state conditions were not attained after incubation for 10 and 20 s, respectively. Assuming that steady-state conditions were achieved after 20 min of labeling for the enamine in E187Q, then from Table IV, setting $A_f = 0.08$ and $A_\infty = 0.20$ yields a first order rate constant of 0.03 s^{-1} in enamine formation. Similarly, for E187A, the first-order rate constant for enamine formation is 0.11 s^{-1} . Errors for the first order rate constants are estimated at $\sim 20\%$. The rates in enamine formation are comparable with rates for substrate turnover of 0.026 and 0.12 s^{-1} measured for mutants E187Q and E187A, respectively. The population stoichiometries for the ketamine $E=$ DG intermediate in the E187Q mutant in Table IV also indicates qualitatively that steady-state conditions were not attained. The inability to displace labeled intermediates following a 20-s chase, even in the presence of a 25-fold isotopic dilution, is significant and contrary to that observed in the wild type enzyme.

Stoichiometries of reaction intermediates derived from incubation against excess labeled DHAP are shown in Table V for the recombinant native and point mutations, E187A and E187Q. The stoichiometries of $E=$ DH and $E=$ D intermediates in the native enzyme concur with reported values (3, 9). The enzymatic fraction of intermediates represented by $E=$ D of 43% is lower than the reported value of 60% (44, 45). Similar studies at 4°C , however, reproduced the reported value of 60% (data not shown). Chase displaced most of the labeled intermediates ruling out significant enzyme heterogeneity and slow interconversion among enzymatic species as a possible cause. Ketamine and enamine populations in the mutant aldolases, based on stoichiometries shown in Table V, are comparable with native enzyme. Different from native enzyme, both mutants showed no significant change in labeled ketamine and enamine populations when chased with excess carrier DHAP.

Structural Analyses—The polypeptide fold of the mutant E187A, E187Q, and K229M monomers was that of an $(\alpha/\beta)_8$ barrel and homologous to native enzyme. The greatest positional differences among the tetramer subunits in the mutant structures occurred among active site residues and C-terminal regions. Structural comparison of mutant structures based on r.m.s. deviation of main-chain atoms from equivalent wild type position showed that E187A exhibited the largest differences with respect to native (0.99\AA) whereas E187Q showed the smallest (0.40\AA). B -factors of the C-terminal region for the residues 344–363 compared with B -factors of the main subunit body were on average six times greater in each mutant whereas the same difference in B -factors was only 3-fold with the native enzyme. The average r.m.s. deviation among equivalent $\text{C}\alpha$ atoms in each subunit, excluding C-terminal regions (residues 344–363), was calculated with the program POLYPOSE (46) and used to assess structural disorder. Pairwise comparison between equivalent atoms in subunits, as well as deviation from mean $\text{C}\alpha$ position, ranks native enzyme with the least disorder (0.25 and 0.15\AA , respectively), followed by E187Q (0.31 , 0.19\AA) and E187A having the greatest structural differences observed with respect to native enzyme (0.66 , 0.40\AA). In all comparisons, values for K229M were only slightly greater with respect to those obtained for E187Q.

E187Q Structure—A significant structural feature, common

TABLE IV

Forward reaction steady state with recombinant aldolases showing stoichiometries of covalent intermediates trapped in the presence of saturation concentration of [^{32}P]Fru-P₂ and chased with cold Fru-P₂ (10 mM)

Full tetramer occupancy by an intermediate would correspond to a maximum stoichiometry of four subunits. Shown in parentheses is duration of forward reaction and that for pulse chase, respectively. *Italics* denote duration of turnover experiments with no pulse chase.

Enzyme	Ketamine Fru-P ₂		Eneamine		Ketamine DHAP	
	Pre-chase	Post-chase	Pre-chase	Post-chase	Pre-chase	Post-chase
Native ^a (3 s, 5 s)	0.16 ± 0.02	<0.01	0.79 ± 0.18	0.09 ± 0.02	0.03 ± 0.05	<0.01
E187A ^b (10 s, 20 s) (1 min)	0.01 ± 0.002 <i>0.02 ± 0.003</i>	0.01 ± 0.001	0.09 ± 0.02 <i>0.14 ± 0.03</i>	0.09 ± 0.02	<0.01 <i><0.01</i>	<0.01
E187Q ^b (20 s, 20 s) (20 min)	0.01 ± 0.002 <i>0.02 ± 0.003</i>	0.02 ± 0.002	0.09 ± 0.02 <i>0.22 ± 0.03</i>	0.09 ± 0.01	<0.01 <i><0.01</i>	<0.01

^a For native recombinant enzyme, 1 mM [^{32}P]Fru-P₂ was used in reaction mixture and chased with 10 mM of cold Fru-P₂.

^b For mutant enzymes, 0.4 mM [^{32}P]Fru-P₂ was used in reaction mixture and chased with 10 mM of cold Fru-P₂.

TABLE V

Stoichiometries of covalent intermediates trapped upon incubation with [^{32}P]DHAP (0.4 mM) and chased with cold DHAP (4 mM) of recombinant aldolases

Full occupancy on the aldolase tetramer would correspond to a maximum stoichiometry of four subunits. Shown in parentheses is the duration of equilibrium reaction and that of pulse chase, respectively.

Enzyme	Ketamine		Eneamine	
	Pre-chase	Post-chase	Pre-chase	Post-chase
Native (20 s, 10 s)	0.17 ± 0.02	0.03 ± 0.01	1.70 ± 0.25	0.26 ± 0.06
E187A (20 s, 10 s)	0.06 ± 0.02	0.05 ± 0.02	0.79 ± 0.20	0.66 ± 0.15
E187Q (20 s, 10 s)	0.16 ± 0.02	0.16 ± 0.03	0.63 ± 0.12	0.78 ± 0.18

to all subunits of this isostructural mutant, were residues Gln-187 and Glu-189, which were within hydrogen bonding distance of each other and is shown for an aldolase subunit in Fig. 3. Hydrogen bonding in the native enzyme between residues Glu-187 and Glu-189 does not occur. The average distance between these residues, shown in Fig. 3, is 2.93 Å in E187Q whereas in native enzyme the distance has increased to 3.97 Å. The hydrogen bond between Gln-187 and Glu-189 and high structural isomorphism of E187Q with native indicates that, if either Glu-187 or Glu-189 were neutral in the native enzyme, the absence in hydrogen bond formation between these residues was not due to steric hindrance in native enzyme. Rather, charge neutralization by Glu-187 → Gln mutation promoted interaction between residues Gln-187 and Glu-189 and indicates that, in the native structure, both Glu-187 and Glu-189 must be negatively charged at pH 7.4. The hydrogen bond in E187Q is further stabilized by interactions between Arg-148 and Glu-189 that are not observed in native enzyme and are shown in Fig. 3.

Active site lysine residues 146 and 229 exhibited extensive variability in side-chain conformations compared with native enzyme. In two subunits, the side-chain orientations of Lys-229 and Lys-146 are different from native enzyme whereas in a third subunit the lysine residues exhibit the same conformation as wild type. In the remaining fourth subunit, respective amines of Lys-146 and Lys-229 are within hydrogen bonding distance as shown in Fig. 4. The hydrogen bonding distance of 2.91 Å differs significantly from 4.9 Å observed in all subunits of the native enzyme. In E187Q subunits where Lys-146 and Lys-229 do not hydrogen bond, interaction between the two residues is indirect and is mediated by hydrogen bonding to intervening water molecules. The side chain of Leu-270, which is adjacent to Lys-229 and shown in Fig. 4, makes close contact with Lys-229 in two subunits. In the subunit exhibiting hydrogen bond formation, Leu-270 approaches within 3.46 Å of Lys-229 whereas in the subunit having lysine side-chain conformations similar to native, the residue is within 3.24 Å of Lys-229.

In the remaining two subunits, contact distance with Lys-229 is 4.3 Å, and Leu-270 conformation is identical to that observed in all subunits of the native enzyme.

In the K229M mutant structure, Leu-270 also makes close contact of 3.54 Å with Met-229 in two subunits. In the remaining subunits, Leu-270 rotamer conformation is similar to that of native and contact with Met-229 side chain is 4.04 Å, slightly shorter than in native enzyme. Close contact between Leu-270 and Met-229 side chains in K229M indicates that conformational changes by these aliphatic side chains are stabilized as a result of hydrophobic interactions.

E187A Structure—Mutation of Glu-187 into an alanine residue has created a cavity in the active site and provoked not only rearrangement of side-chain conformations of immediate active site residues but also that of backbone. The r.m.s. deviation from mean subunit position was largest for β-barrel strand residues, 270–273, proximal to Lys-229. Ser-271 backbone amides exhibited largest positional difference (1.4 Å) whereas the Leu-270 side chain showed the greatest rotameric disorder. The backbone disorder is consistent with the presence of two conformationally mobile glycine residues, Gly-272 and Gly-273, in the sequence, which together with Ser-271 bind the DHAP phosphate in the native structure (17). In three of the four subunits, a water molecule was located in each subunit within hydrogen bonding distance of Glu-189 (Wat-1377, Wat-2658, and Wat-3490) and which occupied the binding locus for the carboxyl moiety of Glu-187 in the native structure. The Wat-1377 binding site is shown in Fig. 5.

Lys-146 and Lys-229 adopt side-chain conformations that are different in each subunit as well as with respect to wild type consistent with greater conformational disorder by these residues in E187A mutant structure. As was observed in the E187Q mutant structure, distances between ammonium groups of Lys-146 and Lys-229 were shorter than distances observed in native (4.9 Å) and in two subunits of E187A, Lys-146 and Lys-229, engaged in hydrogen bond formation. In one subunit, Lys-229 Nζ points toward its proper carbonyl group and the cavity created by the E187A mutation making very close contact with Leu-270 side chain (3.01 Å) while participating in hydrogen bond formation with Lys-146. In both subunits where Lys-146 hydrogen bonds with Lys-229, dual conformations were observed for Lys-146 and only one conformation participated in hydrogen bonding. In the alternate conformations, Lys-146 hydrogen-bonded to other active site residues and water molecules similar to the native structure. A close contact was also observed between Leu-270 and Lys-229 Nζ (3.38 Å) in a subunit where Lys-229 did not participate in hydrogen bond formation.

C-terminal Region (Residues 344–363)—r.m.s. deviations of

FIG. 3. Stereoview of electron density showing Gln-187, Glu-189, and Arg-148 residues in the active site of the E187Q mutant structure. The mutant structure is shown superimposed with equivalent residues in the native enzyme (dark green). Gln-187 donates a hydrogen bond to Glu-189 in E187Q whereas Arg-148 makes additional hydrogen bonds with Glu-189 in E187Q not observed in the native structure. Wat-1376 makes a hydrogen bond to Glu-189 whereas Wat-1647 interacts with Glu-189 and Wat-1856. Electron density shown correspond to a $2F_o - F_c$ omit map of residue Gln-187 and contoured at the 1σ level.

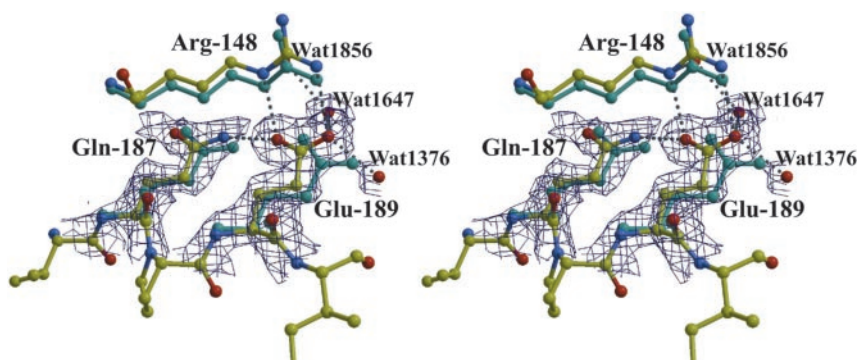


FIG. 4. Stereoview of electron density showing superposition of Lys-146, Gln-187, Lys-229, and Leu-270 in E187Q mutant with equivalent residues in the native enzyme (dark green). The hydrogen bond between lysine residues requires that one lysine residue acts as hydrogen bond acceptor. Glu-187 in the native structure is situated within hydrogen bonding distance between the two lysine residues. Wat-8272 makes hydrogen bonds to Lys-146 and Wat-8338 whereas Leu-270 makes close contact with Lys-229. Electron densities shown correspond to a $2F_o - F_c$ omit map of residues Lys-146 and Lys-229 and contoured at the 1σ level.

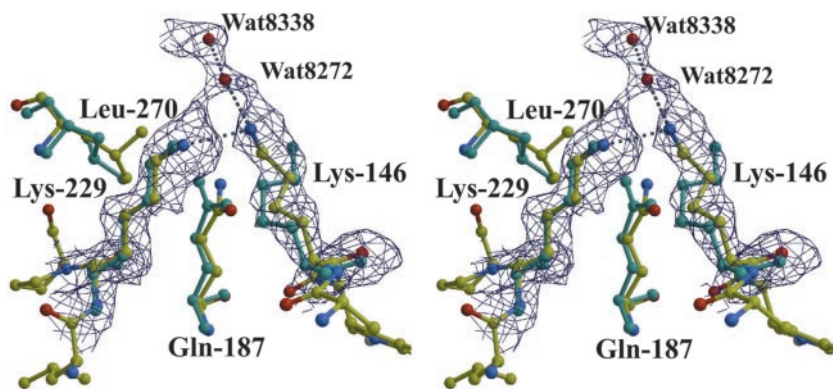
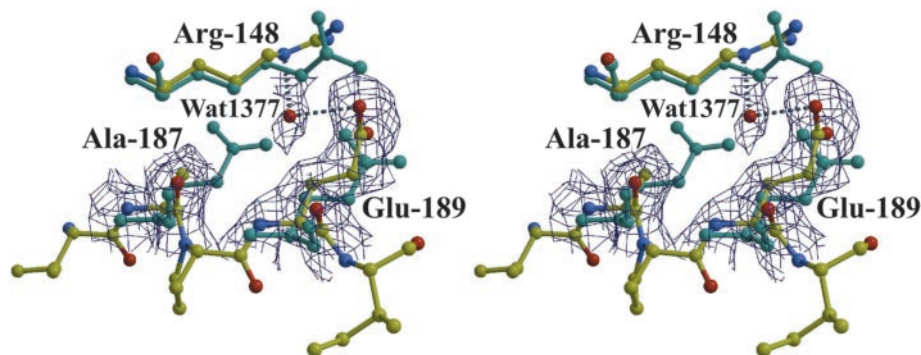


FIG. 5. Stereoview of electron density showing Ala-187, Glu-189, and Arg-148 residues in the active site of the E187A mutant structure and the alanine cavity filled by water molecule Wat-1377. The mutant structure is shown superimposed with equivalent residues in the native enzyme (dark green). Wat-1377 hydrogen bonds Arg-148 and Glu-189 in the E187A mutant structure whereas Arg-148, contrary to native structure, does not hydrogen bond with Glu-189. Electron density shown corresponds to a $2F_o - F_c$ omit map of residue Ala-187 and Wat-1377 and contoured at the 1σ level.



the C-terminal region backbone of the mutant structures, E187A, E187Q and K229M, calculated with respect to native were 3.95, 2.77, and 2.21 Å, respectively. These large deviations from mean square positions, compared with deviations of 0.77, 0.28, and 0.34 Å, respectively, when using only β -barrel core coordinates, residues 1–343, indicate significant conformational heterogeneity and are consistent with C-terminal region flexibility. The largest conformational variability invariably occurred for the traces of the C-terminal regions in the two subunits whose C terminus tyrosine residues were not anchored at the subunit interface of an adjacent tetramer. These C-terminal regions nevertheless folded as in native structure toward their respective active sites. In the native structure, conformations of these C-terminal regions stabilized DHAP binding in the active site (17). In the mutant structures, the same C-terminal regions did not interact with active site residues, nor was there evidence for active site binding.

DISCUSSION

Point mutations at active site residues Glu-187 and Lys-229 in rabbit muscle aldolase did not compromise subunit polypeptide folding, and each mutant retained full structural integrity. Of the three mutant structures, the largest positional differ-

ences were observed in the non-isosteric point mutation E187A with respect to native enzyme structure. The cavity created in the active site by the alanine substitution in this mutant induced minor structural perturbations, which were distributed throughout the polypeptide backbone in each subunit. In the isosteric mutants, E187Q and K229M, structural variations were confined primarily to the level of side-chain conformations with respect to native enzyme. The high structural isomorphism displayed by each mutant aldolase with native enzyme makes perturbations in structural integrity an unlikely explanation for the observed functional differences. In fact, the mutant E187A, which exhibited the largest positional disorder with respect to native, possessed higher catalytic activity than mutant E187Q, which had least structural differences with respect to native.

The basis for the enhanced activity by E187A with respect to E187Q is phenotypic in origin. The mutation to alanine produced a cavity at the former carboxylate locus that created a binding site for a water molecule (shown in Fig. 5). Hydrogen bonding with Glu-189, located at the active periphery, stabilizes the water molecule and allows Glu-189 as a conjugate base to activate the water molecule. The inverse solvent isotope effect, observed for the E187A mutant, is indeed consistent

with participation of OH^- in the reaction mechanism. Furthermore, OH^- is a stronger nucleophile than a carboxamide moiety, correlating with the higher observed activity by E187A mutant compared with E187Q.

Glu-187 and Glu-189 Act As a Proton Bridge—The substantial loss in catalytic activity over the entire pH range in each of the physiologically neutral Glu-187 mutations, seen in Fig. 2*b*, is consistent with a functional role involving proton transfer by Glu-187. In the isosteric E187Q mutant, hydrogen bonding between Gln-187 and Glu-189 involves slight mutual side-chain adjustment where, with respect to native enzyme, Glu-189 carboxylate displaces by 1.2 Å and Gln-187 carboxamide by 0.6 Å toward each other and indicates that in native enzyme, either Glu-187 or Glu-189, in acid form, could prompt proton transfer by small readjustments of carboxylate side chains. The slightly greater displacement by Glu-189 is stabilized through additional interactions with Arg-148 not present in native enzyme. Although the carboxamide moiety of Gln-187 is a weaker base than the carboxylate function of Glu-187, its capacity to participate in hydrogen bond formation is very similar (47). The absence of hydrogen bonding between the two glutamate residues in the native structure indicates that Glu-187 and Glu-189 exist in their respective conjugate bases. A conjugate base, within potential hydrogen bonding distance of the Lys-229 amine, would allow Glu-187 to participate in proton transfers at the level of the reaction mechanism.

The increase observed in the kinetic solvent isotope effect by E189A with respect to native, shown in Table II, is consistent with proton transfers in the transition state involving solvation catalytic proton bridges (43). In all mutant structures as well as native, Glu-189 is extensively solvated and participates in hydrogen bonds with solvent molecules. The cavity created by the carboxylate side-chain loss due to the alanine mutation would allow a water molecule to interact directly with Glu-187. Solvation catalytic proton bridges consisting of an acidic donor-acceptor pair such as Glu-187 and H_2O are consistent with models proposed (48), if the water molecule participating in the catalytic hydrogen bond does not exchange readily with other solvent molecules. The binding locus for Wat-1377, shown in Fig. 5 for mutant E187A, could provide an advantageous attachment site in E189A for a water molecule by allowing it to hydrogen-bond not only with Glu-187 but also Arg-148, which would simultaneously sequester and align it for efficient proton transfer. The negligible reduction in catalytic activity for E189A mutation over the entire pH range, seen in Fig. 2*c*, indicates that the acidic donor-solvent pair compensates efficiently for loss of carboxylate functionality and implies that a significant fraction of Glu-187 is present in the conjugate base form between pH 5 and 10. The extensive solvation of Glu-189 at the subunit surface argues against a pK_a increase by Glu-189, especially given Glu-189 hydrogen bonding with Arg-148 in the native structure, which would serve to stabilize a negative charge on the residue. A significant fraction of Glu-187 and Glu-189 ionized over pH range 5–10 corroborates the structural data where Glu-187 and Glu-189 are fully ionized at pH 7.4 (pH of crystallization buffer). Acidic pK_a values allows Glu-187 and Glu-189 to function as a catalytic proton bridge throughout the pH range 5–10.

The reduction in catalytic activity by the isosteric mutant E189Q, which cannot be compensated for by pH, shown in Fig. 2*c*, further supports a proton transfer role for Glu-189. Although the carboxamide side chain of Gln-189 has a similar capacity to participate in hydrogen bond formation as a carboxylate moiety, because it is a weaker base (49), the mutation would compromise proton transfers with solvent and Glu-187. Furthermore, by analogy with E187Q, hydrogen bonding be-

tween Glu-187 and Gln-189 in E189Q could hinder access by water molecules to Glu-187 affecting catalytic activity. A proton bridge function by the two residues would explain the unusual presence of glutamate residues that are within hydrogen bonding distance of each other in class I eucaryotic aldolases, yet neither of these are protonated. Proton transfer, being an extremely fast reaction, would ensure a preponderance of the Glu-187 conjugate base form throughout the catalytic cycle in native enzyme.

Bond Cleavage and Intermediate Formation—The calculated rates of enamine formation from the Fru- P_2 imine do not significantly differ from turnover rates for both Glu-187 mutants and are consistent with C_3 – C_4 bond cleavage or preceding steps rate-limiting in the forward direction. Steady-state oxidation levels in the presence of Fru- P_2 also concur with C_3 – C_4 bond cleavage or the preceding steps that are rate-limiting in Glu-187 mutants. DHAP equilibrium oxidation levels, which do not depend on C_3 – C_4 bond cleavage, although reduced in the Glu-187 mutants, are not rate-limiting thereby eliminating the necessity for having common rate steps of Schiff base and enamine formation rate-limiting. Although the ketamine populations in both Glu-187 mutants are small in Table IV, accumulation of ketamines was detectable and further supports that a subsequent step and not a preceding step has become rate-limiting in the forward direction. The data are consistent with the interpretation that C_3 – C_4 bond cleavage has become rate-limiting in Glu-187 mutants.

Cleavage of the C_3 – C_4 bond depends on proton abstraction of the C_4 hydroxyl to initiate substrate rearrangement and requires a base on the enzyme to act as proton acceptor. The loss of carboxylate functionality in the Glu-187 mutants, thereby making substrate cleavage rate-limiting, strongly argues that Glu-187 is indeed the base responsible for proton abstraction during C–C bond cleavage. The proton bridge would ensure that Glu-187 is present in conjugate base form, subsequent to ketamine intermediate formation, allowing it to fulfill such a role. The Glu-187 role in catalyzing C–C bond cleavage would exclude such a role postulated for Asp-33 (18), which is located on the side opposite to both Glu-187 and Lys-229 in the active site. The oxidation data do not exclude that common rate steps in Schiff base formation may also be compromised in both Glu-187 mutants, because steady-state as well as DHAP equilibrium oxidation rates are reduced in these mutants. General base catalysis by a glutamate residue in Schiff base formation has been observed in bacterial KDPG aldolase where nucleophilic activation of the Schiff base forming lysine also involves a neighboring active site glutamate residue (25).

The loss of proton transfer capability by the neutralizing point mutations E187Q and E187A significantly perturbed pH activity profiles (Fig. 2, *b* and *c*) and indicates significant pH dependence by the reaction mechanism in the native enzyme (Fig. 2*a*) on the ionization constant of Glu-187. The implication of Glu-187 in several microscopic rate steps that involve proton transfers is consistent with an activity profile sensitive to pH. Indeed, the acidic limb of the pH activity profile for the native enzyme corresponds to a macroscopic $\text{pK}_a = 5.1$, in agreement with the pK_a expected for a glutamate residue, and coherent with Glu-187 as the titrated residue. The fully ionized state of Glu-187 at pH 7.4, deduced from the structural data, further supports such an interpretation and suggests that any pK_a shifts due to hydrophobicity of the active site microenvironment are likely to be small or negligible.

Hydrogen Bond between Lys-146 and Lys-229 in Glu-187 Mutants—Hydrogen bonding between the amines of Lys-229 and Lys-146 requires that one of the lysine residues be no longer protonated at pH 7.4. Lys-146 is exposed and solvated in

the active site, seen in Fig. 4, whereas Lys-229 is located deeper in the β -barrel center where it is less solvated and is surrounded by apolar and hydrophobic residues suggesting that Lys-229 must be the neutral residue. The close interaction of Lys-229 with Leu-270, not seen in native enzyme and shown in Fig. 4, further supports that Lys-229 may be neutral, because an unprotonated lysine exhibits greater hydrophobicity than a charged lysine (50) and hence would be preferred in interaction with hydrophobic residues such as Leu-270. The conformational envelope of Lys-229 is thus consistent with Lys-229 being unprotonated in at least half of the subunits in both mutants and implying a pK_a of 7.4 or lower.

The proximity of Glu-187 to both Lys-146 and Lys-229, shown in Fig. 4, would allow a negative charge on Glu-187 to stabilize positive charges on both Lys-146 and Lys-229 through ion pairing. In the native crystal structure, the lysine residues are far apart, 4.9 Å, and Lys-229 does not make close contact with Leu-270 supporting the interpretation that Glu-187, by stabilizing protonation of both Lys-146 and Lys-229, prevents their hydrogen bonding with each other. Inactivation studies indicate a pK_a of 8.5 for Lys-146 in the native enzyme (51), and consistency with the structural data would then imply a Lys-229 $pK_a \geq 7.5$. Hence, in the absence of charge stabilization by Glu-187, Lys-146 destabilizes the Lys-229 positive charge permitting hydrogen bonding with each other as well as Lys-229 interaction with Leu-270 in the Glu-187 mutant structures.

Evidence that charge destabilization modifies lysine pK_a has been demonstrated in acetoacetate decarboxylase from *Clostridium acetobutylicum* where such electrostatics ensures Schiff base formation under acidic conditions. The enzyme catalyzes the decarboxylation of acetoacetate via Schiff base intermediate formed between substrate and Lys-115 (52), and whose pK_a has been determined as 6 (53). Mutagenesis experiments have shown that neutralization of an adjacent Lys-116 increases the pK_a of Lys-115 by >3.2 units, substantially compromising catalytic activity at pH 6 (7). Although the structure of acetoacetate decarboxylase from *C. acetobutylicum* has not been determined, the data strongly support the aforementioned conclusion that, in the absence of electrostatic screening, charge destabilization by an adjacent lysine residue such as Lys-146 provokes a decrease in the Schiff base forming lysine pK_a .

Point mutations in rabbit muscle aldolase that neutralize Lys-146, such as K146M and K146A, diminish catalytic activity by five orders of magnitude (20, 22) and result in extremely slow ketamine formation at pH 7.5, whereas steady-state intermediate levels were not significantly compromised compared with native enzyme (20). Slow ketamine formation in neutral Lys-146 mutants would be consistent with a charge on Lys-229 no longer being screened by that on Lys-146 promoting formation of a zwitterionic pair, Lys-229/Glu-187 and reducing the concentration of Lys-229 nucleophile. Significant steady-state levels would not be inconsistent with similar formation of zwitterionic pairs between the various cationic ketamines and Glu-187.

Ligand Dissociation—Insignificant displacement of radiolabeled intermediates by cold label in Glu-187 mutants, seen in Tables IV and V, would suggest that apparent ligand off-rates are slower compared with internal microscopic rate steps. Indeed, both DHAP and Fru-P₂ release from their respective Michaelis complexes are rate-limiting in the native enzyme under steady-state conditions (3). Although very slow ligand release in the Glu-187 mutants could explain the inability to displace intermediate populations in the presence of excess carrier, structural isomorphism of the Glu-187 mutants with respect to native enzyme would argue against conformational

effects provoking very slow label displacement from Michaelis complexes. Rather, very slow exchange in both Fru-P₂- and DHAP-labeled intermediates suggests that common rate steps in the breakdown of both labeled intermediates have been compromised in Glu-187 mutations. Ligand exchange for both types of labeled intermediates depends on prior ketamine hydrolysis, hence the very slow observed exchange implies inhibition in breakdown of the protonated imine-3 and/or its carbinolamine precursors, 1 and 2.

The slow exchange of ketamine intermediates in Glu-187 mutants is consistent with electrostatic stabilization of ketamine intermediates by Glu-187 and suggests an additional proton transfer role for Glu-187. A pK_a of 7.4 or lower for Lys-229 in Glu-187 mutants would not require nucleophilic activation for carbinolamine formation. However, electrostatic destabilization by Lys-146 of the positive charge on the dipolar carbinolamine-1 and protonated imine-3 would result in label being preferentially trapped as the neutral carbinolamine-2 and/or neutral imine in Glu-187 mutants. The neutral imine is, however, not on the main reaction trajectory, and if it were to represent a significant off-pathway reaction, it should result in accumulation of both Fru-P₂- and DHAP-labeled ketamine intermediates with respect to native enzyme, which is not observed. An inability to protonate 2 due to Glu-187 mutations would, however, severely compromise formation of the dipolar carbinolamine-1 and result in a very slow ligand off-rate. A proton transfer role for Glu-187 in carbinolamine formation would be consistent with its postulated role in nucleophilic activation of Lys-229 as it invokes proton exchange with the same chemical moiety, namely Lys-229 N ζ .

Reaction Mechanism—Glu-187 fulfills several roles in the catalytic cycle of muscle aldolase. Glu-187 by virtue of its central position in the active site allows it to screen protonated ketamine intermediates on Lys-229 from the positive charge on Lys-146 at physiological pH thereby enhancing their stability. The Glu-187 and Glu-189 catalytic proton bridge ensures rapid proton transfer and thus the preponderance of Glu-187 in conjugate base form throughout the catalytic cycle, enabling it to abstract the proton from the O₄ hydroxyl during substrate cleavage. The positive charge on Lys-146 or that of cationic intermediates formed on Lys-229 reciprocally stabilize the conjugate base form of Glu-187 as well as the negative charge developing on O₄ during proton abstraction. A $pK_a \leq 7.4$ for Lys-229 in Glu-187 mutants alludes to, because of electrostatic screening by Glu-187, a basic pK_a in the native enzyme and is consistent with the proton transfer role proposed for Glu-187 in nucleophilic activation of Lys-229 as well as in carbinolamine formation.

The additional interactions between Glu-189 and conserved Arg-148, observed in the E187Q structure compared with native enzyme, shown in Fig. 3, optimize hydrogen bonding between Glu-189 and Glu-187 and would in the native enzyme align the protonated state of Glu-187 with Glu-189 for optimal proton transfer. However, by stabilizing the negative charge on Glu-189, the positive charge on Arg-148 could hinder proton transfer with Glu-187. The postulated role of Arg-148 in mediating Fru-P₂ C₆-phosphate binding in rabbit muscle aldolase (24) and the observation in rabbit liver aldolase, where C₆-phosphate interacts with Arg-148² is consistent with at least partial dissociation of Arg-148/Glu-189 interaction during substrate binding. Transient dissociation of the Arg-148/Glu-189 ionic pair by active site events could gate and facilitate transfers along the proton bridge. The absence of the C₆-phosphate in Fru-1-P, which results in a 40-fold loss in activity, due in part to a 6-fold reduction in Schiff base formation (30), would not be inconsistent with such an interpretation.

Aldolase Structure Function—The extensive functional role for Glu-187 in the reaction mechanism of mammalian aldolases is in agreement with the structural evidence derived from a carbinolamine complex in *Escherichia coli* KDPG aldolase (25). In the latter aldolase, conserved Glu-45 is the only general base in the active site and is situated within hydrogen bonding distance of the Schiff base forming Lys-133. Glu-45 thus plays a multifunctional role mediating proton transfer during catalysis that includes nucleophilic activation leading to carbinolamine formation, proton abstraction in C–C bond cleavage, and proton exchange with the enamine intermediate. Superposition of the two aldolase β -barrel structures based on the folding order of the polypeptide strands comprising the β -barrel preserves only the spatial alignment of the conserved lysine in the active sites of the two aldolases; the respective conserved glutamates being located on different strands (data not shown). In *E. coli* transaldolase B structure, whose polypeptide sequence also displays a β -barrel fold, superposition resulted in spatial alignment of Glu-96 and Schiff base forming Lys-132 with that of Glu-187 and Lys-229, respectively, in muscle aldolase (21). Glu-96, whose function has not been investigated, is conserved in transaldolases and is situated within hydrogen bonding distance of Lys-132 on the adjacent strand as in muscle aldolase. The spatial dispositions of other active site residues resulting from the structure superpositions are dissimilar among the three enzymes suggesting that the aldolase active sites arose from a β -barrel ancestor bearing a common lysine residue. The permutation of the conserved glutamate position highlights an evolutionary paradigm of divergent evolution enabling aldolases, folding as β -barrel structures, to accommodate differences in substrate specificity whereas ensuring a proton transfer capability about the essential lysine residue. General base catalysis by a glutamate residue appears to be an indispensable feature in Schiff base forming aldolases responsible for carbohydrate metabolism.

Acknowledgment—Critical discussions with Dr. C. Blonski, CNRS, Toulouse are gratefully acknowledged.

REFERENCES

- Rose, I. A., O'Connell, E. L., and Mehler, A. H. (1965) *J. Biol. Chem.* **240**, 1758–1765
- Rutter, W. J. (1964) *Fed. Proc. Fed. Am. Soc. Exp. Biol.* **23**, 1248–1257
- Rose, I. A., Warms, J. V. B., and Kuo, J. D. (1987) *J. Biol. Chem.* **262**, 692–701
- Rose, I. A., and Warms, J. V. B. (1985) *Biochemistry* **24**, 3952–3957
- Grazi, E., Rowley, P. T., Cheng, T., Tchola, O., and Horecker, B. L. (1962) *Biochem. Biophys. Res. Commun.* **9**, 38–43
- Ray, B. D., Harper, E. T., and Fife, W. K. (1983) *J. Am. Chem. Soc.* **105**, 3731–3732
- Highbarger, L. A., Gerlt, J. A., and Kenyon, G. L. (1996) *Biochemistry* **35**, 41–46
- Avigad, G., and England, S. (1972) *Arch. Biochem. Biophys.* **158**, 337–346
- Kuo, D. J., and Rose, I. A. (1985) *Biochemistry* **24**, 3947–3952
- Syngusch, J., Beaudry, D., and Allaire, M. (1987) *Proc. Natl. Acad. Sci. U. S. A.* **84**, 7846–7850
- Gamblin, S. J., Davies, G. J., Grimes, J. M., Jackson, R. M., Littlechild, J. A., and Watson, H. C. (1991) *J. Mol. Biol.* **219**, 573–576
- Hester, G., Brenner-Holzach, O., Rossi, F. A., Struck-Donatz, M., Winterhalter, K. H., Smith, J. D. G., and Piontek, K. (1991) *FEBS Lett.* **292**, 237–242
- Kim, H., Certa, U., Dobeli, H., Jakob, P., and Hol, W. G. (1998) *Biochemistry* **37**, 4388–4396
- Chudzick, D. M., Michels, P. A., de Walque, S., and Hol, W. G. (2000) *J. Mol. Biol.* **300**, 697–707
- Kelley, P. M., and Tolan, D. R. (1986) *Plant Physiol.* **82**, 1076–1081
- Anai, M., Lai, C. Y., and Horecker, B. L. (1973) *Arch. Biochem. Biophys.* **156**, 712–719
- Blom, N., and Syngusch, J. (1997) *Nat. Struct. Biol.* **4**, 36–39
- Morris, A. J., and Tolan, D. R. (1993) *J. Biol. Chem.* **268**, 1095–1100
- Morris, A. J., Davenport, C. R., and Tolan, D. R. (1996) *Protein Eng.* **9**, 61–67
- Morris, A. J., and Tolan, D. R. (1994) *Biochemistry* **33**, 12291–12297
- Jia, J., Huang, W., Schorken, U., Sahn, H., Sprenger, G. A., Lindqvist, Y., and Schneider, G. (1996) *Structure* **4**, 715–724
- Blonski, C., Demoissac, D., Périé, J., and Syngusch, J. (1997) *Biochem. J.* **323**, 71–77
- Dalby, A., Dauter, Z., and Littlechild, J. A. (1999) *Protein Sci.* **8**, 291–297
- Choi, K. H., Mazurkie, A. S., Morris, A. J., Utheza, D., Tolan, D. R., and Allen, K. N. (1999) *Biochemistry* **38**, 12655–12664
- Allard, J., Grolchulski, P., and Syngusch, J. (2001) *Proc. Natl. Acad. Sci. U. S. A.* **98**, 3679–3684
- Berthiaume, L., Tolan, D. R., and Syngusch, J. (1993) *J. Biol. Chem.* **268**, 10826–10835
- Racker, E. (1952) *J. Biol. Chem.* **196**, 347–351
- Healy, M. J., and Christen, P. (1973) *Biochemistry* **12**, 35–41
- Berenblum, I., and Chain, E. (1938) *Biochem. J.* **32**, 295
- Model, P., Ponticorvo, L., and Rittenberg, D. (1968) *Biochemistry* **7**, 1339–1347
- Syngusch, J., Coulombe, R., Cassanto, J. M., Sportiello, M. G., and Todd, P. (1996) *J. Cryst. Growth* **162**, 167–172
- Howard, A. J. (1990) *XGEN User Guide*, Version 1.0, Burlington, MA
- Brunger, A. T., Krukowski, A., and Erickson, J. W. (1990) *Acta Crystallogr. Sect. A* **46**, 585–593
- Jones, T. A., Zou, J. Y., Cowan, S. W., and Kjeldgaard, M. (1991) *Acta Crystallogr.* **47**, 110–119
- Kleywegt, G. J., and Jones, T. A. (1997) *Methods Enzymol.* **277**, 208–230
- Blom, N. S., and Syngusch, J. (1998) *Acta Crystallogr. Sect. D Biol. Crystallogr.* **54**, 461–466
- Kleywegt, G. J., and Brunger, A. T. (1996) *Structure* **4**, 897–904
- Esnouf, R. M. (1999) *Acta Crystallogr. Sect. D Biol. Crystallogr.* **55**, 938–940
- Merritt, E. A., and Murphy, M. E. P. (1994) *Acta Crystallogr. Sect. D Biol. Crystallogr.* **50**, 869–873
- Laskowski, R. A., MacArthur, M. W., Moss, D. S., and Thornton, J. M. (1993) *J. Appl. Crystallogr.* **26**, 283–291
- Grazi, E. (1975) *Biochem. J.* **151**, 167–172
- Cook, P. F. (1991) *Enzyme Mechanism from Isotope Effects*, CRC Press, Boca Raton, FL, pp. 81–82
- Cook, P. F. (1991) *Enzyme Mechanism from Isotope Effects*, CRC Press, Boca Raton, FL, pp. 85–86
- Grazi, E., and Trombetta, G. (1978) *Biochem. J.* **175**, 361–365
- Iyengar, R., and Rose, I. A. (1981) *Biochemistry* **20**, 1223–1229
- Diamond, R. (1992) *Protein Sci.* **1**, 1279–1287
- Pollack, R. M., Kayser, R. H., and Damewood, J. R., Jr. (1977) *J. Am. Chem. Soc.* **99**, 8232–8237
- Kreevoy, M. M., and Liang, T. M. (1980) *J. Am. Chem. Soc.* **102**, 3315–3322
- Pine, S. H. (1987) *Organic Chemistry*, 5th Ed., McGraw-Hill, New York, p. 100
- Creighton, T. E. (1983) *Proteins: Structures and Molecular Properties*, W. H. Freeman, New York, p. 150
- Hartman, F. C., and Brown, J. P. (1976) *J. Biol. Chem.* **251**, 3057–3062
- Warren, S., Zerner, B., and Westheimer, F. H. (1966) *Biochemistry* **5**, 817–823
- Schmidt, D. E., and Westheimer, F. H. (1971) *Biochemistry* **10**, 1249–1253